Theory of the fundamental vibration-rotation-translation spectrum of H_2 in a C_{60} lattice

Roger M. Herman*
104 Davey Laboratory, Department of Physics, Pennsylvania State University, University Park, Pennsylvania 16802, USA

John Courtenay Lewis†
Department of Physics and Physical Oceanography, Memorial University of Newfoundland, St. John's Newfoundland and Labrador, Canada A1B 3X7

(Received 5 October 2005; published 7 April 2006)

Calculations are presented for the fundamental vibration-rotation spectrum of H_2 in fcc C_{60} (fullerite) lattices. The principal features are identified as lattice-shifted "vibration-rotation-translation" state absorption transitions. The level spacings of the H_2 modes are calculated numerically for the potential function resulting from the summation of the individual C-H_2 potentials for all C atoms in the six nearest neighbor C_{60} molecules. The potential is approximately separable in Cartesian coordinates, giving a very good approximation to exactly calculated translational energies for the lower levels. The positions and relative strengths of the individual transitions are calculated from the eigenfunctions for this separable potential. The line shapes are assumed to be Lorentzian, and the widths are chosen so as to give good fits to the DRIFT spectrum of FitzGerald *et al.* [Phys. Rev. B **65**, 140302(R) (2002)]. A theory of the C-H_2 induced dipole moment is developed with which to calculate intensities. In order to fit the observed DRIFTS transition frequencies it is found necessary to take the overlap part of the C-H_2 potential to be about 13% longer in range than the C-H_2 potential in graphene. Furthermore, differences in the theoretical spectra obtained with a near-optimal exp-6 potential and near-optimal Lennard-Jones 12-6 potential are clearly evident, with the exp-6 potential giving a better fit to observation than the Lennard-Jones potential. Similarly, Lorentzian line shapes assumed for the individual transitions yield better agreement with observation than Gaussian line shapes.

DOI: 10.1103/PhysRevB.73.155408 PACS number(s): 68.43.Pq, 78.30.Na, 33.20.Ea

I. INTRODUCTION

The search for an efficient low-pressure high-density storage system for molecular hydrogen has led to study of several hydrogen-adsorbing nanostructures.[2] These offer the potential of providing safe, efficient hydrogen storage for onboard use in vehicles, which most likely would employ fuel cells for the clean generation of electrical power using H_2 as fuel. With that in mind, it is necessary to understand the interactions of H_2 with carbon nanostructures of all types. One of the most basic of these nanostructures might be bundles of carbon nanotubes, for example.

Excellent infrared spectra of the H_2 fundamental band for the trapped molecules have recently been obtained by diffuse reflectance infrared Fourier transform spectroscopy (DRIFTS).[1] It is the primary purpose of this paper to analyze these spectra and to deduce as much as possible about the fundamental carbon atom interactions with H_2.

A progress report on our work as of June 2004 was published earlier.[3] Theoretical considerations relating to spectra of H_2 in interstitial channels (ICs) in carbon nanotube bundles were presented in earlier work.[4]

H_2 of course does not have a permanent dipole in isolation, but its interactions with other molecules can induce dipole moments which give rise to observable optical transitions. Spectra arising from transition dipoles induced in interactions between small atoms and molecules, H_2 in particular, have been extensively studied.[5] Our overall approach is to place the C_{60}-H_2 DRIFT spectra in the context of these well-known interaction-induced spectra.

The C_{60} lattice is known to be fcc at room temperature,[6] this modification being known as "fullerite." Hydrogen can easily diffuse into these lattices within two or three hours at room temperature.[1,7] The radius of a C_{60} molecule is $a = 3.551$ Å. The nearest-neighbor separation in fullerite lattices is 10.023 Å. The octahedral sites are defined by the six nearest-neighbor C_{60} molecules, equidistant from the center of the site on orthogonal axes. The equilibrium distance of each C_{60} from the center of an octahedral site is $d = 7.087$ Å. There is one octahedral site per C_{60} molecule. In addition there exist two tetrahedral sites per C_{60} molecule in which the H_2 molecule would be surrounded by four equidistant C_{60} molecules in tetrahedral symmetry, each at a distance of 6.138 Å from the H_2 equilibrium position. Hydrogen in these tetrahedral sites has a higher ground state energy than in the octahedral sites, so that the tetrahedral sites are found not to be important in the present analysis due to their small probability of occupation, in accord with previous findings from a neutron scattering study.[7] Nonetheless the tetrahedral sites appear to be important *dynamically* in the loading and unloading of the fullerite lattice.[8]

The DRIFT spectrum of fullerite saturated with H_2 is shown in all five figures in this paper. We are in agreement with the identification of the spectral features provided by FitzGerald *et al.*,[1] following the ~ -54 cm^{-1} shift mentioned below. In the most intense parts of the spectrum, the translational states undergo a simultaneous jump with the vibrational and rotational states. The major features of the spectrum can be labeled as follows, which is standard in the field of interaction induced H_2 spectroscopy:

$$Q(J)_R: \quad J \to J, \quad n_z \to (n_z + 1)$$

$$Q(J)_P: \quad J \to J, \quad n_z \to (n_z - 1)$$

$$S(J)_R: \quad J \to (J+2), \quad n_z \to (n_z+1)$$

$$S(J)_P: \quad J \to (J+2), \quad n_z \to (n_z-1)$$

$$O(J)_R: \quad J \to (J-2), \quad n_z \to (n_z+1)$$

$$O(J)_P: \quad J \to (J-2), \quad n_z \to (n_z-1).$$

A weak band around 3800 cm^{-1} arising from the $O(2)_P$ and $O(3)_R$ transitions is expected, but presumably is obscured by noise in the published spectrum. The larger $O(2)_R$ intensity will be hidden by the $Q(J)_P$ peaks, for all J, at 3950 cm^{-1}. The tallest peak, at 4200 cm^{-1} arises from the $Q(J)_R$ transitions, for all J. This peak also contains, in its higher frequency wing, the $S(0)_P$ feature. The peak at 4550 cm^{-1} is mostly $S(1)_P$, also supplemented by the weaker $S(0)_R$. The tall peak at 4800 cm^{-1} is mostly $S(1)_R$, and it hides the $S(2)_P$ feature. The small peak at 5000 cm^{-1} is mostly $S(2)_R$, but has the $S(3)_P$ in its high frequency wing. The weak peak at 5200 cm^{-1} is almost entirely $S(3)_R$. The reason for the predominance of the $S(1)$ over the $S(0)$ features comes not only from the larger statistical weight of the $J=1$ states over $J=0$, but by virtue of the spin statistics, the $S=1$ state that accompanies odd-J states being three times as frequently encountered, all other things equal, as the singlet spin state accompanying the even-J states.

In Sec. III we discuss the C-H_2 and C_{60}-H_2 interaction potential. In Sec. IV we will describe the H_2 translational states and energies. On the basis of our calculations we argue that the C-H_2 potential in C_{60}-H_2 is significantly different from its form in graphene-H_2. In Sec. V we examine the induced transition dipole moments, basing the deduction of interaction induced dipoles on the well known interactions for the He-H_2 system, suitably generalized through known or plausible rules to the C-H_2 system and hence, by integration to C_{60}-H_2 interactions. Finally, in Sec. VI we will discuss the calculation of the spectral intensities. The DRIFT spectrum of FitzGerald *et al.* gives relative but not absolute intensities. Hence we have freely adjusted the intensity scales for our theoretical spectra in Figs. 1–5 to give the best agreement with the DRIFTS.

II. NOTATION

In most of this paper we report lengths in Å, energies in meV, and frequencies in cm^{-1}. However, the available data for induced dipole moments[5,9] and polarizabilities[10] have been reported in atomic units (a.u.). For that reason, in much of Secs. IV–VI we use a.u., for which the length is the Bohr radius, $a_0=0.5292$ Å, the unit dipole moment is $1ea_0$ and the unit polarizability is $1(ea_0)/(e/a_0^2)=a_0^3$. The energy unit in atomic units is the hartree: 1 hartree$=e^2/a_0=27.21$ eV.

For an octahedral site we specify the location of the H_2 in Cartesian coordinates as x, y, z, where the coordinate axes pass through the centers of the C_{60} molecules which bound the site. These centers hence are located at $(\pm d,0,0)$, $(0,\pm d,0)$, and $(0,0,\pm d)$. The vector from one H nucleus of H_2 to the other is $\mathbf{s}=(s,\vartheta,\varphi)$. The vector from the center of mass of H_2 to a carbon atom we write as $\mathbf{r}=(r,\theta,\phi)$, while the vector from the center of mass of H_2 to the center of a C_{60} molecule we write as $\mathbf{R}=(R,\Theta,\Phi)$.

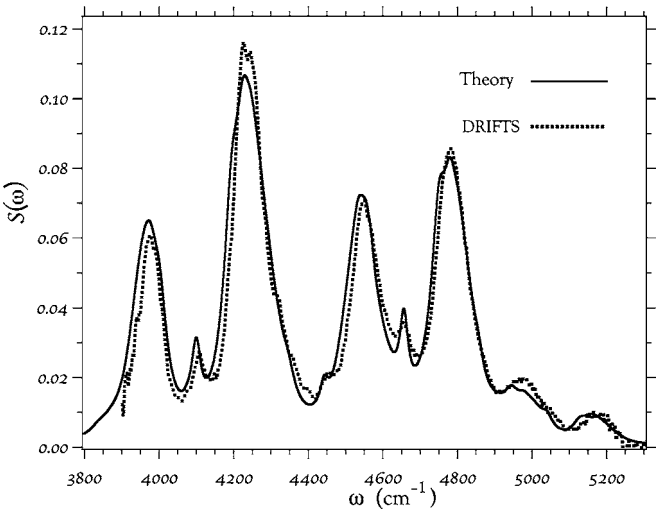

FIG. 1. DRIFTS and our best theoretical spectrum for the fundamental band of H_2 in a fullerite lattice as a function of the frequency ω. The theoretical spectrum was calculated for the exp-6 potential for which $\sigma=3.22$ Å and $\varepsilon=3.25$ meV. The principal component Lorentzian line shapes have HWHH of 24 cm^{-1}. Other parameters are described in the text.

The interaction potential of an individual carbon atom in graphene or fullerite with H_2 we write as $U_{\text{C-H}_2}(r)$ while $U_{\text{C}_{60}\text{-H}_2}(R)$ is the interaction potential of H_2 with a C_{60} molecule. We denote the net potential of H_2 at x,y,z in an octahedral site as $V(x,y,z)$.

The exp-6 potential with the same well depth ε, the same zero crossing σ and the same value of the C_6 coefficient as the Lennard-Jones 12-6 potential

$$U(r) = 4\varepsilon\left[\left(\frac{\sigma}{r}\right)^{12} - \left(\frac{\sigma}{r}\right)^{6}\right] \tag{1}$$

is given by

$$U(r) = 4\varepsilon\left[\exp[-\beta(r-\sigma)] - \left(\frac{\sigma}{r}\right)^{6}\right] \tag{2}$$

with

$$\beta = 11.2912/\sigma. \tag{3}$$

III. THE C-H_2 POTENTIAL

The interaction potential between C atoms and H_2 is presently well understood for the C atoms composing a graphite sample, this being based upon the analysis of selective adsorption data in H_2-graphite surface scattering.[11] The interaction potential can be represented to good accuracy using a Lennard-Jones 12-6 potential of the form of Eq. (1) with σ being as usual the separation at which $U(R)_{\text{C-H}_2}=0$, and ε being the well depth. According to Novaco,[11] $\sigma=2.85$ Å while $\varepsilon=4.11$ meV (47.7 K).

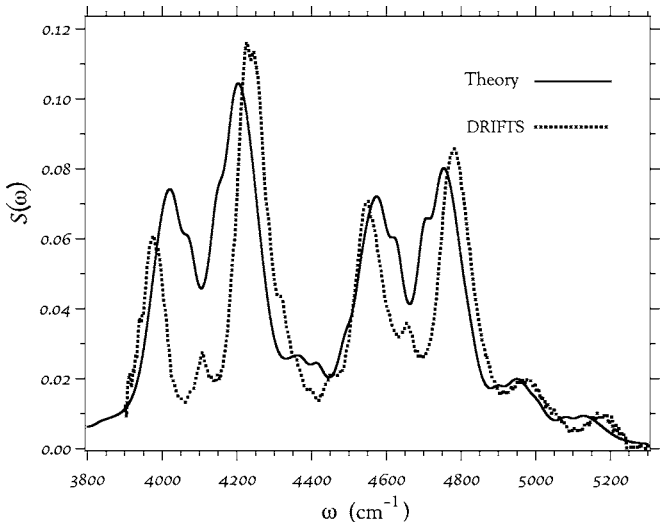

FIG. 2. Theoretical spectrum using an exp-6 potential based on the known C-H_2 potential in graphene, for which σ=2.85 Å and ε=4.11 meV; with DRIFTS.

When this potential is averaged over a graphene plane, assuming the carbon atoms to be smeared uniformly over the plane, the result is

$$U_{\text{graphene}}(z) = N_C \sigma^2 \varepsilon \left[0.4\left(\frac{\sigma}{z}\right)^{10} - \left(\frac{\sigma}{z}\right)^4 \right], \tag{4}$$

where z is the distance from the graphene plane to the H_2 center of mass, and N_C is the number density of the C atoms in the graphene plane (N_C=0.3821 Å^{-2}=0.107a_0^{-2}). Electrostatic interactions between the individual carbon-carbon bonds and the permanent quadrupole moment of H_2 are either negligible or are subsumed into the Lennard-Jones form, as are induction energies.

We consistently have found that for calculating the spectrum the Lennard-Jones form of the C-H_2 potential is inferior to the exp-6 form, in which the short range part of the potential has exponential dependency on the molecular separation. For the graphene-H_2 interaction, the observed states in selective absorption are sufficiently low-lying that this refinement would have negligible consequences. We are therefore justified in assuming an exp-6 form of the interaction having the same hard-sphere separation σ and well depth ε as the Lennard-Jones potential of Eq. (1).

It is tempting to apply the Novaco graphene-C-H_2 potential directly to the C_{60}-H_2 interaction. And in fact, we began our analysis of the DRIFT spectrum in just this way. It soon became clear (the results being shown in Fig. 2) that the interaction parameters per C atom in C_{60} molecules are quite different from those for C atoms in graphene. A C_{60} molecule is simply not a graphene layer wrapped around a sphere:[12] the double bonds all point away from the vertices of the pentagons in the surface, thus preventing the resonant alternation in double bond positions that is so important in graphene layers and indeed in aromatic compounds. It is, in fact, well known[12] that C_{60} and C_{70} are decidedly nonaromatic in their chemistry.

Because of the relatively high translational energies of the H_2 molecules within the confines of the C_{60} lattice sites of octagonal symmetry, the details of the anharmonicities become far more important than they were in the H_2 selective absorption spectra of H_2 with graphite. As such, it is necessary to find some means of dealing with the parameters of the exp-6 potential that will be assumed for C_{60}-H_2 individual C-H_2 interactions. For this purpose, let us first consider the He-H_2 interactions which have been exhaustively investigated by Schaefer and Kohler[13] within the context of Eqs. (2) and (3). From their potential it is found that σ =3.00 Å=5.67a_0 and ε=1.18 meV. From this value of σ we obtain β=3.7632 Å^{-1}=1.9914a_0^{-1}. The resulting exp-6 potential gives an excellent approximation to the numerical results of Schaefer and Kohler throughout the domain of greatest importance for the present problem, namely $0.75\sigma < r < 1.25\sigma$, with the largest errors being $\leqslant$5% in the steep short range region. Similar potential energy functions for other interacting atoms would then take the same form, with different values of σ (and therefore β) and ε.

Short range forces come about from charge overlap and Fermi repulsion, and will operate similarly in a large variety of cases. Hence the rule expressed in Eq. (3) should relate the short range noncovalent forces among small molecules to good approximation. If we apply this rule to the Ar-H_2 interaction, for example, we predict a β value of 3.555a_0^{-1} as compared with the value given by LeRoy and Carlin[14] of 3.5955a_0^{-1}, representing a difference of 1%, despite the large overall difference from the He-H_2 interaction. Thus we can conclude that this will, in all likelihood, provide us with a realistic β value. In the interest of time, we shall not consider other β values in this work, carrying on with just this one manner of choosing β to obtain the exp-6 interaction for any given choice of σ and ε.

When the right-hand side of Eq. (1) is summed over the C atoms of a C_{60} molecule the result is

$$U_{C_{60}\text{-}H_2}(R) = 30\varepsilon \frac{\sigma^2}{Ra}\left[\frac{2}{5}\left(\frac{\sigma}{R-a}\right)^{10} - \frac{15}{2}\left(\frac{\sigma}{R-a}\right)^4 + \frac{15}{2}\left(\frac{\sigma}{R+a}\right)^4 \right] \tag{5}$$

with R being the H_2 displacement from the center of the C_{60} molecule. In the actual fullerite lattice the C_{60} molecules will be somewhat deformed from perfect truncated icosahedra. We will ignore these distortions, and will assume uniform smearing of the C atoms over a sphere of radius a. Equation (5) is analogous to Eq. (4), and is obtained from analogous assumptions.

When the right-hand side of Eq. (2) is summed in the same way the result is[7]

$$U_{C_{60}\text{-}H_2}(R) = 4.00\frac{\varepsilon}{Ra}\left[\frac{30}{\beta^2}[1+\beta(R-a)]e^{-\beta(R-a-\sigma)} - \left(\frac{15\sigma^2}{2}\right)\left(\frac{\sigma}{R-a}\right)^4 + \left(\frac{15\sigma^2}{2}\right)\left(\frac{\sigma}{R+a}\right)^4 \right]. \tag{6}$$

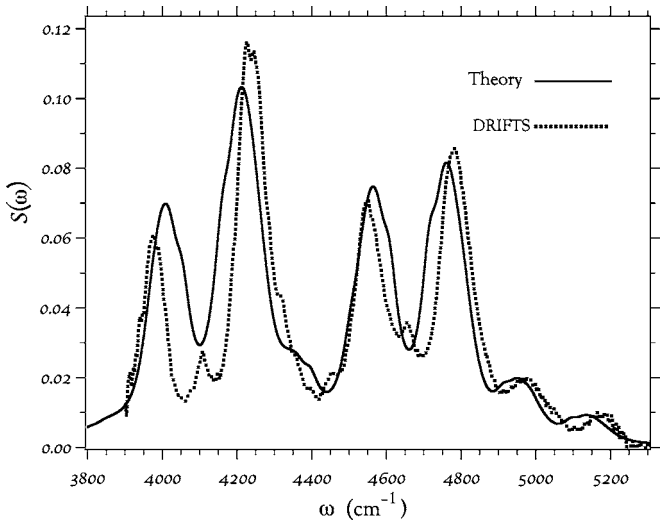

FIG. 3. Theoretical spectrum using the exp-6 form of the Wang *et al.*[15] potential (σ=2.97 Å and ε=3.69 meV), with DRIFTS.

The resulting exp-6 potentials that we consider are softer than the Lennard-Jones for smaller separations, while providing the minima at slightly greater distances (1.1339σ) than the Lennard-Jones values of $2^{1/6}\sigma=1.1225\sigma$. In the case of graphene we find the C-H_2 exp-6 potential as given by Eq. (2) to have parameters with ε=4.11 meV, $\beta=2.096a_0^{-1}$ =3.96 Å^{-1}, and σ=2.85 Å=$5.386a_0$, which leads to the theoretical spectrum shown in Fig. 2. In view of the obvious deficiencies in that theoretical spectrum, it seemed a larger value of σ appeared to be indicated. Hence it seemed reasonable to try the potential parameters of Wang *et al.*,[15] for which σ=2.97 Å and ε=3.69 meV (42.8 K). The resultant spectrum for the corresponding exp-6 potential is shown in Fig. 3. It is seen that this theoretical spectrum is similar to that of Fig. 2, though the agreement with the DRIFT spectrum is considerably improved. For this reason, we felt encouraged to try even larger values of σ, with our best result being shown in Fig. 1 for σ=3.22 Å (hence β=3.5066 Å^{-1}) and ε=3.25 meV.

Finally, FitzGerald *et al.*[7] and Yildrim and Harris[16] have proposed a C-H_2 potential, which they have used with success in analyzing neutron scattering data, based upon the two H atoms interacting independently as spherical entities with the C atom. Each C-H potential is of exp-6 form, characterized by σ=3.18 Å, ε=1.488 meV, and β=3.67 Å^{-1}. Their prescription leads to a C-H_2 potential which is approximately represented by the exp-6 form with $\sigma_{\text{C-H}_2}$=3.28 Å, $\varepsilon_{\text{C-H}_2}$ =2.68 meV and $\beta_{\text{C-H}_2}$=3.667 Å^{-1}. Thus, their value of σ is quite comparable to our best value, while their ε is somewhat less and β somewhat greater than our best values. The latter might be expected to give rather higher and more separated translational state energies. The resulting spectrum indeed shows this, giving translational state features that are too broad and too highly separated from the corresponding translation-free positions.

In all of our calculations we have neglected the anisotropic C-H_2 interactions. They are identically zero at the octahedral site itself and have zero expectation value for the lowest translational state for H_2 about the octahedral site, by virtue of the symmetry about that site. Also, they have no permanent value for the lowest rotational state of H_2. They will, however, give small splittings in the energies for higher rotational-translational states. These again are relatively small, and therefore are accommodated through the linewidths ascribed to the individual transitions.

A feature which is much more influential than the anisotropy of the C-H_2 interaction is the internal vibrational dependence of the interaction potential. By noting that in He-H_2 there is a dependence of $U(R)$ upon the atomic separation within H_2,[13] the theory of Herman and Short[17] could be used to obtain an estimate of the internal vibrational dependence of $U(R)$. In He-H_2, this amounts to about a 6% higher interaction energy per vibrational excitation within H_2, for the long range part of the potential, which is the dominant part along the bottom of the well. The dependence of the Ar-H_2 interaction potential upon the internuclear separation within H_2 as calculated by LeRoy and Carlin[14] leads to an almost identical behavior to that of He-H_2 in this regard. Because of the rather high interaction energies between H_2 and the C_{60} lattice, this vibrational effect will account for the approximately -54 cm^{-1} overall shift in the positions of the major features of the spectrum relative to what might be expected without this effect. This shift will figure prominently in the calculation of the spectrum, not only by virtue of the shift of the whole spectrum, but also in the relative shifts in position of the individual translational components within the overall spectrum.

IV. TRANSLATIONAL EIGENSTATES AND ENERGIES

The total potential function governing the translational states of H_2 in an octahedral site is given by the sum of its interactions with the six nearest-neighbor C_{60} molecules, if ternary induction effects are neglected. The three-dimensional structure of this potential is rather complicated in form, and there is no system of coordinates in which it is exactly separable.

Therefore a computer code has been developed for obtaining numerically the eigenstates and energies with the exact three-dimensional Hamiltonian. The code uses a discrete variable representation method (DVR) as described in an earlier publication.[3] The eigenstates themselves are difficult to work with, and we have therefore sought a simplified way of representing the states in an approximate manner. In examining the eigenenergy spectrum for the exact potential, we discovered that the exact spectrum was approximately that of a separable potential in Cartesian coordinates. This discovery, that the eigenproblem was approximately that of a separable system, greatly facilitated the calculation of line intensities.

Yildrim and Harris[16] also have found eigenstates and energies beginning with an approximate separable potential, which they write in spherical polar coordinates, based upon their C-H_2 potential, described above. The difference in our approaches lies in the fact that they begin with wave functions in a spherical basis, then perturb with the exact octrahedral symmetry Hamiltonian to obtain very large shifts in

reaching the first order result. In our approach, we separate in Cartesian coordinates, then similarly perturb with the exact octahedral Hamiltonian to obtain an approximation to the exact spectrum; but we notice that in this basis, the perturbations are minor. That discovery allowed us to take the Cartesian basis states as good approximations to the actual eigenstates. This, in turn, greatly facilitated the calculation of the spectra, in that for z polarization, say, the only transitions of consequence are those for which $n_z \rightarrow n_z \pm 1$.

To describe in detail how we obtain the system energy levels, let us begin by defining a one-dimensional potential $V_{1D}(x)$ as the superposition of two potentials fo the type given by Eq. (6), with $R=d\pm x$, thus

$$V_{1\mathrm{D}}(x) = U_{\mathrm{C_{60}\text{-}H_2}}(d+x) + U_{\mathrm{C_{60}\text{-}H_2}}(d-x), \tag{7}$$

where d is the equilibrium separation between the H_2 and the C_{60} molecules and x is the displacement of H_2 along the x axis. $V_{1\mathrm{D}}(x)$ is approximately equal to the exact potential along the x axis

$$V_{1\mathrm{D}}(x) \simeq V(x,0,0) - \frac{2}{3}V(0,0,0). \tag{8}$$

$V_{1\mathrm{D}}(x)$ is decidedly anharmonic, even exhibiting double minima for reasonable choices of σ and ε in the C-H_2 potential. The one-dimensional energies E_n can be labeled with $n=0,1,2,\ldots$ corresponding to one-dimensional eigenstates being ψ_0, ψ_1, etc.

As stated above, we have found that to a good approximation the exact low-lying eigenenergies were sums of the one-dimensional eigenenergies to an excellent approximation. Thus

$$V(x,y,z) \simeq V_{1\mathrm{D}}(x) + V_{1\mathrm{D}}(y) + V_{1\mathrm{D}}(z) \tag{9}$$

and

$$E^{\mathrm{exact}}_{n_x n_y n_z} \simeq E_{n_x} + E_{n_y} + E_{n_z} \tag{10}$$

reproduces the exact eigenvalue structure fairly accurately, as is shown in Table I.

Because the E_n are numerically identical for the x,y,z directions, the energy of the (310) state (for example) can be written as

$$E_{310} = E_3 + E_1 + E_0, \tag{11}$$

with quantum numbers 3,1,0 being permutable in any fashion.

The approximate eigenstates can be represented by the product of the one-dimensional anharmonic wave functions,

$$\psi_{n_x n_y n_z}(x,y,z) \simeq \psi_{n_x}(x)\psi_{n_y}(y)\psi_{n_z}(z), \tag{12}$$

the right-hand side of which we will usually represent as $|n_x n_y n_z\rangle$. We do not at present have a means to assess Eq. (12) quantitatively other than by the eigenenergies that it leads to. However, for the present purpose of estimating relative rather than absolute spectroscopic line strengths it is reasonable to expect the transition dipole matrix elements calculated on its basis to bear the proper ratios with one another.

The first six one-dimensional energy levels E_n are shown in Table II, together with the energy differences between successive levels. It is these energy differences which, in the separation model, give the translational contributions to the band frequencies. These one-dimensional energies were obtained by a shooting/matching procedure, as stated above. They serve as a check on the accuracy of our three-dimensional DVR procedure. Thus $E_{0\,0\,0}$ as calculated by the DVR procedure for the separable three-dimensional potential is $-932.080\,11\ \mathrm{cm}^{-1}$ (Table I) while $3E_0 = -932.080\,18\ \mathrm{cm}^{-1}$ from values in Table II; and $E_{0\,1\,4} = -314.137\,23\ \mathrm{cm}^{-1}$ as calculated by the DVR method, while $E_0+E_1+E_4 = -314.178\,44\ \mathrm{cm}^{-1}$ according to Table II.

This shows the known tendency of the DVR method to decrease in accuracy with increasing quantum number. As the energy levels for the full three-dimensional potential are calculated in the same way as those for the sum potential, this comparison also serves to indicate the accuracy of these energy levels.

The difference

$$V(x,y,z) - V_{1D}(x) + V_{1D}(y) + V_{1D}(z) \tag{13}$$

is not separable but is of octahedral symmetry. This leads to splittings in the exact energies which are not present in the sum-potential energies. For example, energy level 4 of Table I has the structure

$$\frac{1}{\sqrt{3}}(|0\,0\,2\rangle + |0\,2\,0\rangle + |2\,0\,0\rangle) \tag{14}$$

to first order, and is split off from and is of lower energy than the doubly degenerate energy level 5, the eigenfunctions of which to first order can be represented as the linear combinations

$$\frac{1}{\sqrt{6}}(2|0\,0\,2\rangle - |2\,0\,0\rangle - |0\,2\,0\rangle)$$

and

$$\frac{1}{\sqrt{2}}(|2\,0\,0\rangle - |0\,2\,0\rangle). \tag{15}$$

These splittings under the influence of the octahedral symmetry group of the exact Hamiltonian are small for the low-lying states, and appear prominently only in the higher states, which will have minor importance in the present problem. The assumed linewidths are thought ultimately to be able to account for the effects of these splittings.

The approximate energies in the separation model are indeed quite close to the exact results (within about 5 cm^{-1} of energies which are on the order of 10^3 cm^{-1}, with the energy spacings of importance in the present spectroscopic problem being even closer to exact). The exact energies can be approached even more closely through adding to each the first order perturbation

$$\Delta E^{(1)}_{n_x\,n_y\,n_z} = \langle n_x n_y n_z | H^{\mathrm{exact}} - H^{\mathrm{approx}} | n_x n_y n_z \rangle. \tag{16}$$

The sum of the energies $(E_{000} + \Delta E^{(1)}_{0\,0\,0})$ gives the variational energy for the approximate ground state, and as such represents an upper limit for the lowest energy. A small correction

TABLE I. The energy levels calculated for the full three-dimensional potential $V(x,y,z)$ together with the energy levels for the sum potential $V(x)+V(y)+V(z)$ of the Cartesian separation as calculated by the DVR method with a one-dimensional basis of 20 (hence a three-dimensional basis of 8000). The first column is the ordinal for each distinct energy, while the second column gives the degeneracy of the energy level. The Cartesian separation states are linear combinations of the states shown in the fifth column. Linear combinations of these states are presumptively the principal states contributing to the corresponding exact three-dimensional wave functions. For the states marked with an asterisk *specific* linear combinations are required, as, for example, in Eq. (15). $E_{0\,0\,0}$ and $E_{0\,1\,4}$ are shown to eight significant figures for purposes of comparision with one-dimensional eigenvalues computed by a shoot-and-match procedure, for which see Table I and text.

Energy level	Degeneracy	Energy for $V(x,y,z)$ cm^{-1}	Energy for sum potential cm^{-1}	Principal states $(n_x n_y n_z)$
1	1	−926.66601	−932.08011	(0 0 0)
2	3	−830.9	−836.4	(0 0 1) and permutations thereof
3	3	−739.4	−740.8	(0 1 1) and permutations thereof
4	1	−714.7	−713.1	(0 0 2)* and permutations thereof
5	2	−705.6	−713.1	Same as above
6	1	−652.3	−645.1	(1 1 1)
7	3	−624.7	−617.5	(0 1 2) and permutations thereof
8	3	−617.5	−617.5	Same as above
9	3	−566.2	−569.9	(0 0 3) and permutations thereof
10	3	−538.3	−521.8	(1 1 2) and permutations thereof
11	1	−513.1	−494.2	(0 2 2)* and permutations thereof
12	2	−501.8	−494.2	Same as above
13	3	−489.7	−474.3	(0 1 3) and permutations thereof
14	3	−474.2	−474.3	Same as above
15	3	−427.2	−409.8	(0 0 4) and permutations thereof
16	1	−419.7	−398.5	(1 2 2)* and permutations thereof
17	2	−408.3	−398.5	Same as above
18	1	−407.8	−378.6	(1 1 3)* and permutations thereof
19	2	−394.1	−378.6	Same as above
20	3	−374.5	−351.0	(0 2 3) and permutations thereof
21	3	−368.6	−351.0	Same as above
22	3	−325.00800	−314.17844	(0 1 4) and permutations thereof
23	3	−324.6	−314.2	Same as above
24	1	−318.8	−275.3	(2 2 2)
25	3	−308.2	−255.3	(1 2 3) and permutations thereof
26	3	−284.5	−255.3	Same as above

to this result can be achieved through second order perturbation theory, in the approximate form

$$\Delta E^{(2)}_{000} \simeq -3\langle 200|H^{\text{exact}}|000\rangle^2/E_2. \tag{17}$$

For our best parameter set we find $\Delta E^{(1)}$ to be +5.44 cm^{-1}, and $\Delta E^{(2)}$ to be −0.001 cm^{-1}, which is negligible. Thus the convergence of the perturbation series seems to be rapid, while the corrected sum potential energy shows excellent agreement with the exact result for the ground state: −925.8 cm^{-1} vs the exact result, −926.7 cm^{-1}.

There are several sources of spectral line splittings that are substantially smaller than those represented by E_1-E_0, for example, which gives the smallest splitting between the successive vibration-rotation-translational transitions in the spectrum. These can arise from the differences between the exact and the separable potential eigenenergies. For instance, the transition $n_z=0\rightarrow n_z=1$ will be manifest spectroscopically as the sum of transitions $(000)\rightarrow(001)$, $(010)\rightarrow(011)$, $(110)\rightarrow(111)$, $(020)\rightarrow(021)$, and so forth; any transition in which n_x and n_y remain constant while $n_z=0\rightarrow n_z=1$ will be included. Because the exact transition energies will in fact be split to greater or lesser degree, each transition in the separation model will in fact represent a comb of transition frequencies. Finally, as mentioned above, we have neglected the translation-rotation coupling which will give rise to line splittings for states in which $J\geqslant 1$ and any of n_x, n_y, or $n_z \geqslant 1$. While these splittings may not always be negligible,

TABLE II. The first six one-dimensional energy levels E_n calculated to eight significant figures, and the energy differences ΔE between successive energies.

n	E_n cm^{-1}	ΔE cm^{-1}
0	−310.69339	
		95.66248
1	−215.03091	
		123.27872
2	−91.75219	
		143.20731
3	51.45512	
		160.13195
4	211.58707	
		175.18389
5	386.77096	

they will be blended by the Lorentzian line shapes (FWHH =48 cm^{-1} in the spectrum of Fig. 1). For this reason, we feel justified in not treating them explicitly in our calculations at this time.

V. THE C-H_2 INTERACTION INDUCED TRANSITION DIPOLES

In this section we use atomic units exclusively, and in that and in other regards follow Frommhold's[5] usage, although not rigorously. The transition dipole operator is regarded as being the induced dipole as a function of static H_2 position within the cage formed by the six nearest-neighbor C_{60} molecules, as well as for fixed internuclear separation within H_2, in the Born–Oppenheimer approximation. Of course there is no permanent dipole for the free H_2 molecule, so one is required to examine the interaction-induced dipoles. To begin, let us consider the general expression of Poll and Hunt[18] for the νth spherical component of the dipole induced in H_2 interacting with a spherical atom,

$$p_\nu(\mathbf{r},\mathbf{s}) = \frac{4\pi}{\sqrt{3}} \sum_{\Lambda LM} A_{\Lambda L}(r,s) C(\Lambda L 1; M(\nu - M)) \times Y_{\Lambda M}(\vartheta,\varphi) Y_{L(\nu-M)}(\theta,\phi). \quad (18)$$

For any given H_2 vibrational transition (such as the $0 \rightarrow 1$ transition considered in this paper) the A functions can be integrated between the corresponding vibrational states in H_2 at the outset, giving for the transition operator for the 0-1 band the effective form

$$p_\nu^{01}(\mathbf{r},\vartheta,\varphi) = \frac{4\pi}{\sqrt{3}} \sum_{\Lambda LM} B_{\Lambda L}^{01}(r) C(\Lambda L 1; M(\nu - M)) \times Y_{\Lambda M}(\vartheta,\varphi) Y_{L(\nu-M)}(\theta,\phi). \quad (19)$$

In this paper we shall consider illumination by randomly polarized light. Therefore, no generality is lost by orienting the six nearest-neighbor C_{60} molecules on the x, y, and z axes, with no averaging over lattice orientations being required. Moreover, one can consider the effects of only the $\nu=0$ dipole component, eventually multiplying by a factor 3 to accomodate the corresponding effects of the $\nu=\pm 1$. So for our purposes,

$$p_0^{01}(\mathbf{r},\vartheta,\varphi) = \frac{4\pi}{\sqrt{3}} \sum_{\Lambda LM} B_{\Lambda L}^{01}(r) C(\Lambda L 1; M, -M) \times Y_{\Lambda M}(\vartheta,\varphi) Y_{L,-M}(\theta,\phi). \quad (20)$$

It is this expression that serves as the starting point for the remaining development in this paper. It remains to sum the above over all C atoms in the C_{60} molecule for given (R,Θ,Φ).

From the symmetry of the H_2 molecule the transition moments $B_{\Lambda L}^{01}$ are nonzero only for even values of Λ and odd values of L. The largest of these transition moments are B_{01}^{01}, which gives rise to $\Delta J=0$ transitions, and B_{23}^{01}, which gives rise to $\Delta J=0, \pm 2$ transitions.

The $B_{\Lambda L}(r)$ functions for the He-HD interaction have been carefully evaluated by Borysow, Frommhold, and Meyer.[9] In He-H_2 the most important of the even-Λ, odd-L terms are almost identical to those in He-HD, however.

All otherwise nonzero terms in Eq. (20) will vanish by symmetry at the origin because they are odd in L. Hence, the dipole can only attain a nonzero value through having displacements from the origin, and these will have opposite sign only when one goes from negative to positive values of the H_2 displacement. Accordingly, H_2 vibration-rotation transitions are allowed only when these are accompanied by translational state changes in which the parity of the z state changes, while the parities of the x and y states remain unchanged. By far the most important of these, for the p_0 operator, are those going from n_z to n_z' states with $n_z' = n_z \pm 1$. In examining the aforementioned paper by Borysow *et al.*, it is evident that the B_{01} term (corresponding to the simplest overlap contribution) dominates at small r, while the quadrupole-induced-dipole term B_{23} dominates at larger r. Thus, we shall work with only those two contributions.

A. The behavior of B_{23} at long range

As already mentioned, B_{23} quantifies the dipole induced by the H_2 quadrupole electrostatic field in the spherical atom. For this reason, it will be proportional to the polarizability of the perturbing atom. If each C atom were to have a simple polarizability α_C, then for the C-H_2 interaction,

$$B_{23}^{01}(r)_{\text{C-H}_2} = \left(\frac{\alpha_C}{\alpha_{He}}\right) B_{23}^{01}(r)_{\text{He-H}_2}. \quad (21)$$

The summation over the 60 C atoms uniformly distributed over the molecular surface of the C_{60} being centered at R,Θ,Φ would then exactly yield the result for the dominant $Y_{20}Y_{30}$ term,

$$p_0^{01}(R,\vartheta,\varphi,\Theta,\Phi) = \frac{4\pi}{\sqrt{3}} C(231;00) B_{23}^{01}(R)_{C_{60}\text{-}H_2} \times Y_{20}(\vartheta,\varphi) Y_{30}(\Theta,\Phi) \quad (22)$$

with

$$B_{23}^{01}(R)_{C_{60}\text{-}H_2} = 60\left(\frac{\alpha_C}{\alpha_{He}}\right) B_{23}^{01}(r=R)_{He\text{-}H_2}. \quad (23)$$

Unfortunately, the C_{60} polarizabilities are not so simple as this picture presents. In carbon compounds it is the individual bonds which act as the seats of polarization, with single and double bonds each having polarization in which the response to the electric field component parallel to the bond is characterized by $\alpha_\parallel$ while that for perpendicular field components will be characterized by $\alpha_\perp$. In C_{60} there are 60 single bonds and 30 double bonds, associated with the 20-hexagon, 12-pentagon structure. In the hexagons, each single bond will form an edge with a pentagon, thereby insuring that there will be 60 of them, while the alternate hexagon bonds will be double. Each of these is shared by a neighboring hexagon, so that in all there will be 20 hexagons with 3 double bonds per hexagon, each double bond being shared by two hexagons, for a total of $(20\times 3)/2=30$ double bonds. It is a fairly good approximation for the long range part of B_{23}^{01} to treat these bonds as uniformly distributed and oriented, and to be concentrated at the center of the C_{60}. In that case,

$$B_{23}^{01}(R)_{C_{60}\text{-}H_2} \simeq f_{C_{60}He} B_{23}^{01}(r=R)_{He\text{-}H_2} \quad (24)$$

at long range, with

$$f_{C_{60}He} = \frac{(60\alpha_{\perp s} + 30\alpha_{\perp d}) + (1/9)[60(\alpha_{\parallel s} - \alpha_{\perp s}) + 30(\alpha_{\parallel d} - \alpha_{\perp d})]}{\alpha_{He}}. \quad (25)$$

The dominant first term is exact for all C_{60}-H_2 separations. The second is exact at very large distances R, and numerical studies have shown it to be nearly exact for the smaller distances encountered in the present problem.

The factor 1/9 arises in Eq. (25) as follows: a factor 1/3 comes from the fact that only one of the three directions is characterized by having a difference from $\alpha_\perp$ given by $(\alpha_\parallel - \alpha_\perp)$; if the field is thought of as being uniform and in the z direction, the parallel component will affect the z component of the dipole through the factor $\sin^2\chi$ where χ is the angle of displacement of an element of surface area from the C_{60} center; the average value of $\sin^2\chi$ then is 2/3; and at a given χ value, on average half of the bond orientations will present only perpendicular directions relative to the field direction, effectively providing a further factor 1/2.

For want of better information, we assume that the bond polarizabilities are those listed by Phillips[10] for single and double C-C bonds in organic molecules, namely $\alpha_{\perp s}=2.6$ a.u., $\alpha_{\parallel s}=9.7$ a.u., $\alpha_{\perp d}=12.7$ a.u., and $\alpha_{\parallel d}=28.6$ a.u., while the He polarizability is well known to be $\alpha_{He}=1.40$ a.u. With these numbers we find that

$$f_{C_{60}He} = 4.55\times 10^2. \quad (26)$$

From Fig. 7 of Borysow *et al.*[9] it is found that

$$B_{23}^{01}(r)_{He\text{-}H_2} = \frac{0.205}{r^4} \quad (27)$$

so that, finally, at long range,

$$B_{23}^{01}(R)_{C_{60}\text{-}H_2} \simeq \frac{93.3}{R^4}. \quad (28)$$

It is Eq. (28) rather than Eq. (23) which should be used in Eq. (22).

The long range (dispersion) part of $B_{01}(r)$ varies as r^{-7} and can be neglected in this problem.

B. Behavior of the induced dipoles at short range

The model for the short range part of the induced transition dipoles that we will use is again taken over from He-H_2 interactions. The basis of our model is that short range forces arise from similar mechanisms regardless of which structures are interacting, as do short range overlap-induced dipoles.

We will begin with B_{01}^{01}. We find, by fitting the graphical data of Borysow *et al.*[9] in the neighborhood of $5.5a_0$, that B_{01}^{01} is given approximately by the expression

$$B_{01}^{01}(r)_{He\text{-}H_2} \simeq 3.15e^{-1.5r}. \quad (29)$$

The overlap dipole is *not* exactly proportional to the force, which itself is approximately

$$F_{s.r.}(r)_{He\text{-}H_2} = 7.966\varepsilon e^{-1.9914(r-\sigma)} \quad (30)$$

$$\simeq 29.1e^{-2.00r}, \quad (31)$$

as follows from fitting the numerical data of Schaeffer and Kohler[13] for He-H_2 between $5.0a_0$ and $5.5a_0$. Comparing Eq. (29) with Eq. (30) it is evident that B_{01}^{01} is of similar functional form to the short range force but is of somewhat longer range. In fact,

$$B_{01}^{01}(r)_{\text{He-H}_2} \simeq 0.271[F_{s.r.}(r)_{\text{He-H}_2}]^{0.75} \tag{32}$$

provided that the numerical values in a.u. are used, as otherwise no meaning can be attached to the 0.75th power of a force. Similarly, from graphical analysis of B_{23}^{01}, after subtraction of the long range part of Eq. (28), the short range part which remains has almost the same functional dependence on r as that of B_{01}^{01}, with a value given by

$$B_{23}^{01} \simeq 0.24 B_{01}^{01}. \tag{33}$$

In sum, while B_{01}^{01} is given in its entirety by Eq. (32), B_{23}^{01} will be given by

$$B_{23}^{01}(r)_{\text{He-H}_2} \simeq 0.0607[F_{s.r.}(r)_{\text{He-H}_2}]^{0.75} + \frac{0.205}{r^4}. \tag{34}$$

We now conjecture that relationship (32) will hold regardless of what other atoms might be interacting with H_2, provided that the bonding is largely physical rather than covalent. In the case of Ar-H_2, we would not be concerned about the larger number of outer shell electrons in Ar, because they enter similarly in producing overlap forces as dipole components, and while there are a greater number of overlap opportunities in Ar than in He, this larger number will also polarize the H_2 molecule in proportion to their number. The one difference that would be of importance is that where overlap is significant, it would be expected that the respective center of overlap polarization would support a charge displacement proportional to the inverse of its ionization potential. Thus, He would give rise to a smaller overlap contribution than if its ionization energy were smaller. We therefore multiply the right-hand side of Eq. (32) by a factor which takes into account the effect of ionization energies, in order to make the relationship applicable to other atom-H_2 configurations. Such a factor might be

$$f_{\text{ionization}}(X\text{-H}_2) = \frac{1/I_{\text{H}_2} - 1/I_{\text{X}}}{1/I_{\text{H}_2} - 1/I_{\text{He}}}. \tag{35}$$

Note that for H_2-H_2 interactions this factor will become zero, as it must by symmetry for the (otherwise) most important dipole component. For the Ar-H_2 interaction, we do have a test, not of the transition dipole, but rather of the dipole expectation values,[9] $B_{01}^{00}(r)$ and $B_{23}^{00}(r)$. The agreements with the functional dependence given by Eq. (30) and Eq. (33) below, utilizing the Ar-H_2 potential of Leroy and Carlin,[14] are reasonable when the above ionization factor is applied, with $I_{\text{H}_2} \simeq 14.5$ eV, $I_{\text{He}} = 24.6$ eV, and $I_{\text{Ar}} = 17.5$ eV. For this combination, B_{23}^{00} strongly dominates B_{01}^{00}, especially at larger distances (those greater than about $6.0a_0$). At the important distance of $5.5a_0$ the values of both B_{23}^{00} and B_{01}^{00} relate properly to one another through Eq. (33) above, and B_{01}^{00} has the expected radial dependence. The radial dependence predicted for B_{23}^{00} appears to be somewhat weaker than is suggested by the graphical data of Borysow *et al.*,[9] however. Note that the ionization energy factor $f_{\text{ionization}}(\text{C-H}_2)$ is actually negative for the C_{60}-H_2 interaction, since the C atoms are presumably more subject to charge displacement than is the H_2 molecule. Its value is found to be −0.390.

Based upon the above considerations and Eq. (6) for the C_{60}-H_2 interaction potential, we find

$$F_{s.r.}(R)_{\text{C}_{60}\text{-H}_2} = \left(30 \times 4.00 \times \frac{\varepsilon}{\beta^2 a}\right) \times \left[-\frac{d}{dR}\left(\frac{1+\beta(R-a)}{R}\right)e^{-\beta(R-a-\sigma)}\right]. \tag{36}$$

With Eqs. (32) and (35) and the ionization factor given above, we find

$$B_{01}^{01}(R)_{\text{C}_{60}\text{-H}_2} = -10.85\gamma\left\{\frac{\varepsilon}{\beta^2 a}e^{\beta\sigma}\left[-\frac{d}{dR}\left(1+\beta\frac{R-a}{R}\right)e^{-\beta(R-a-\sigma)}\right]\right\}^{0.75} \tag{37}$$

with $B_{23}^{01}(r)$ given, for all distances, by

$$B_{23}^{01}(R) = 0.24 B_{01}^{01}(R) + \frac{93.9}{R^4}. \tag{38}$$

The dimensionless factor γ in Eq. (37), and implicitly in Eq. (38), is an adjustable parameter representing our imprecise knowledge of both the short range part and the long range part (through imprecise knowledge of the bond polarizabilities in C_{60}) of the induced dipole components. It is important in that the ratio of the two tallest peaks in the spectrum depend rather sensitively upon it. For our best spectrum its value was chosen as 1.00, but for other parameters, the spectra are optimized for different values, typically not too different from unity.

VI. CALCULATION OF SPECTRAL INTENSITIES

A. The translational transitions

Our calculations are based on the separability approximation following from Eq. (9). With the dipole transition operators specified by Eqs. (37) and (38) it is possible to sum the dipoles as induced by all six neighboring C_{60} molecules, then evaluate the transition matrix elements between the various vibration-rotation-translation states of H_2 within the lattice sites, being careful to weight by the normalized Boltzmann factors of the initial states. As a simplification, for the transitions $(n_x n_y n_z) \rightarrow (n_x, n_y, n_z \pm 1)$, which are by far the most important (and the only ones we have considered), the sums of the Boltzmann-weighted matrix elements of the p_0^{01} operator squared, can be replaced by the classical canonical average on the x and y motions, in the separable limit. We define

$$Z_{3\text{D}} = \sum_{n_x n_y n_z} e^{-E_{n_x n_y n_z}/k_B T} \tag{39}$$

and

$$Q_{3\text{D}} = \int dxdydz e^{-V(x,y,z)/k_B T} \tag{40}$$

to be the three-dimensional quantum mechanical partition function and the classical three-dimensional configurational partition function, respectively, together with

$$Z=\sum_n e^{-E_n/k_BT} \quad \text{and} \quad Q=\int dx e^{-V_{1D}(x)/k_BT} \tag{41}$$

as the corresponding one-dimensional partition function and one-dimensional configurational partition function, respectively. The intensity for all transitions from $n_z \rightarrow n_z \pm 1$ is given by

$$\sum_{n_x,n_y} T(n_z \rightarrow n_z \pm 1) = Z^{-2} \sum_{n_x,n_y} |\langle n_x,n_y,n_z|p_0^{01}(x,y,z)|n_x,n_y,n_z \pm 1\rangle|^2 e^{-(E_{n_x}+E_{n_y})/k_BT} \tag{42}$$

in the separable approximation.

Because double transition matrix elements will be very small the sum over n_x, n_y can then be approximated by a sum involving off-diagonal matrix elements, and this quadruple sum can be expressed as a trace over wave functions on x, y:

$$\begin{aligned}\sum_{n_x,n_y} |\langle n_x,n_y,n_z|p_0^{01}(x,y,z)|n_x,n_y,n_z \pm 1\rangle|^2 e^{-E_{n_x}+E_{n_y}/k_BT} &\simeq \sum_{n_x,n_y}\sum_{n_x',n_y'} e^{-E_{n_x}+E_{n_y}/k_BT}\langle n_x,n_y|\langle n_z|p_0^{01}(x,y,z)|n_z \pm 1\rangle|n_x',n_y'\rangle \\ &\times\langle n_x',n_y'|\langle n_z \pm 1|p_0^{01}(x,y,z)^*|n_z\rangle|n_x,n_y\rangle \\ &= \mathrm{tr}_{x,y}\{|\langle n_z|p_0^{01}(x,y,z)|n_z \pm 1\rangle|^2 e^{-H(x,y)/k_BT}\}.\end{aligned} \tag{43}$$

Replacing the quantum mechanical canonical average over x, y by the classical canonical average we obtain

$$Z^{-2}\mathrm{tr}_{x,y}|\langle n_z|p_0^{01}(x,y,z)|n_z \pm 1\rangle|^2 e^{-H(x,y)/k_BT} = Q^{-2}\int dxdy e^{-V_{2D}(x,y)/k_BT}|\langle n_z|p_0^{01}(x,y,z)|n_z \pm 1\rangle|^2, \tag{44}$$

where

$$H(x,y) = -\frac{\hbar^2}{2m_{H_2}}\left\{\frac{\partial^2}{\partial x^2}+\frac{\partial^2}{\partial y^2}\right\} + V_{2D}(x,y) \quad \text{and} \quad V_{2D}(x,y) = V_{1D}(x) + V_{1D}(y). \tag{45}$$

Because p_0^{01} does not depend on momentum, the momentum contributions to the classical canonical average cancel between numerator and denominator on the right-hand side of Eq. (44). Overall we find that

$$\sum_{n_x,n_y} T(n_z \rightarrow n_z \pm 1) \simeq Q^{-2}\int dxdy e^{-V_{2D}(x,y)/k_BT}|\langle n_z|p_0^{01}(x,y,z)|n_z \pm 1\rangle|^2. \tag{46}$$

It is the latter expression which we use to calculate intensities.

The approximation of Eq. (42) by Eq. (46) is reminiscent of the Born-Oppenheimer separation, in which the nuclei of a molecule are treated as being momentarily at rest while the electrons move in their static electric field. The present approximation, however, is distinctly different from this. Here the z motions are not slower than the x and y motions. Rather, this approximation is based upon two assumptions: first, that simultaneous translational transitions, in which both n_z and either of n_x or n_y change, are relatively infrequent; and, second, that there are enough thermally populated n_z states that the classical approximation Eq. (44) is valid.

Of course, Eq. (46) must be weighted by the normalized Boltzmann factors for the initial rotational-translational states. Even with this simplification, the calculation is still lengthy, but straightforward. As already mentioned, there is a lowering of the internal translational potential energy by 6%, for the upper states ($v=1$) in the transitions. This is the value for He-H_2, and we are assuming that it is unchanged for all physical bonding situations. Thus, the vibrational perturbation for the $v=0,1$ states, summed over all C atoms in the six nearest-neighbor C_{60} molecules, can be represented by the perturbation Hamiltonian

$$H' = 0.06V(x,y,z)\delta_{v,1}. \tag{47}$$

It is this effect that leads to the spectral shifts of about 54 cm^{-1} from the corresponding free molecule vibration-rotation energies observed by FitzGerald and his colleagues.[1] Strictly speaking, the excited state translational wave functions should be defined and calculated relative to this altered potential. We did indeed use first order perturbation theory to obtain translational state-dependent eigenenergies which were included in the calculation. But these had little effect aside from that noted above (additionally causing a slight spreading of the translational R features and narrowing of the corresponding P features). In view of this, we felt that corresponding refinements in the transition dipoles would be too small to justify the increase in computational complexity.

In evaluating the transition dipole matrix elements, the short range parts of B_{23}, along with B_{01} have been multiplied by a factor γ, which represents the degree to which, as mentioned above, we may not have been able to assess accurately the ratio of long range to short range dipole contributions; either could contain errors based upon our lack of good information at the present time, or due to errors in modeling the short range contributions. For those cases of serious interest, the parameter γ has a value nearly equal to unity. But the parameter must be kept because it is important in determining the ratio of the two largest peak heights in the spectrum, namely the $Q(J)_R$ and $S(1)_R$ peaks. It is important to note that because of the $Y_{\Lambda M}(\vartheta,\varphi)$ dependences of the B_{01} and B_{23} dipole components, the B_{01} component gives rise only to Q transitions. By contrast, the B_{23} component produces quadrupolar transition type selection rules, giving $\Delta J=0$ (but not $J=0 \rightarrow J=0$) Q transitions, as well as the $\Delta J=+2$ [$S(J)$ features] and $\Delta J=-2$ [$O(J)$ features].

B. The "sharks' teeth"

In addition to the broad principal peaks in the spectrum, there are three small sharp features at approximately 4100, 4450, and 4650 cm^{-1} in the spectra of FitzGerald *et al.*[1]

These represent $Q(J)$, $S(0)$, and $S(1)$ features, which have no apparent translational splittings, lying at their natural positions, though shifted by the characteristic approximately -54 cm^{-1}. These must arise from H_2 molecules within the C_{60} sample, but located at sites that do not have the octahedral symmetry which, as we have seen, forbids the induction of a "permanent" induced dipole at the central position. There are four possible sources for such dipole generation. First, FitzGerald and his collaborators have considered at length the possibility that through the rotational motions of the C_{60} molecules strict octahedral symmetry will be lost by the fact that inequivalent parts of the C_{60} structures may lie on opposite sides of the H_2 molecules. This mechanism has the characteristic feature that below $T_0=260$ K the C_{60} rotational motions freeze out,[6] presumably leaving all H_2 molecules in sites of strict octahedral symmetry. This would correspond to the observed[1] decrease in the sharks'-teeth intensities below T_0. This interpretation of the spectra is complicated by the fact that the transition at 260 K is also a structural phase transition, from an fcc lattice to a simple cubic one.

However, there are three other possibilities which should be considered. One is that H_2 could lie in tetrahedral sites, of which there are two per C_{60} molecule in the fcc lattice. Here there would be a comparatively large induced dipole, but the energies of the H_2 translational states within the tetrahedral locations are high enough to ensure that this situation is so improbable that the resulting sharks'-teeth intensities simply would be too small to account for the observed intensities, in accordance with previous work.[7,8] The third possibility is that H_2 will be adsorbed into surface sites, which will be similar to the octahedral sites, except that each such site will lack an endcap C_{60} molecule. The H_2 will then necessarily see a very large deviation from octahedral symmetry, which will lead to a sizeable induced dipole at its equilibrium location. Finally, similar dipoles would be induced whenever two H_2 molecules would occupy adjacent defective octahedral sites within the crystal, defective specifically in that the C_{60} between them were missing. The resulting dipole for each would be about as large, due to the loss of octahedral symmetry, as for the H_2 molecule in a pore site. We assume that the H_2 molecules in question are bonded in an equivalent manner to their bonding in the octahedral site, with dipole induction due only to the unbalanced C_{60} molecule on the z axis. Using only the dominant B_{23}^{01} component of the induced dipole moment it is found that $\langle p^2\rangle = 8.567\times10^{-6}$ a.u., with the fractional number of equivalently bonded sites being 0.0756.

VII. CALCULATED SPECTRA

For reference, we have calculated the spectrum in the manner described above for the exp-6 potential based upon the Lennard-Jones parameters $\sigma=2.85$ Å and $\varepsilon=4.11$ meV inferred from H_2 selective adsorption experiments and inelastic neutron scattering spectra.[11,18–20] The spectrum calculated with this potential is shown in Fig. 2. The results for the corresponding Lennard-Jones potential are about the same. We note the rather poor agreement, to the extent that we did not attempt to include the small sharks' teeth in the calculation. We next tried the exp-6 potential based upon the somewhat larger value of σ proposed by Wang *et al.*[15] and used in a recent study[21] of Raman spectra of hydrogens adsorbed on nanotubes, for which $\sigma=2.97$ Å (about 4% larger than for C-H_2 in graphene), $\varepsilon=3.69$ meV and β given through Eq. (3) as $\beta=2.012a_0^{-1}=3.802$ Å^{-1}. This potential improves agreement with experiment, as shown in Fig. 3. Again, the small features are omitted for comparison, as with Fig. 2. Had they been included, the agreement with experiment would have been lessened. Those cases gave us some hope, nonetheless, that one could explain the spectra by using even larger values of σ, within the exp-6 potential. The result of our search is shown in Fig. 1 where the solid (theory) curve shows somewhat remarkable agreement with the DRIFTS data. For this figure σ and ε were chosen to be $\sigma=3.22$ Å, $\varepsilon=3.25$ meV, with β again chosen in accordance with Eq. (3). For this spectrum, γ was chosen as 1.00, with 7.6% of the H_2 molecules lying in the open surface channels, or in sites having missing C_{60} vacancies. Even though the spectra so obtained are quite good, and might be thought to serve to pin down the values of σ and ε rather closely (perhaps to within 1% or so) there are some difficulties, which will be noted below, which prevent us from definitively stating the values of these parameters. Rather, the parameters should be regarded as being somewhat tentative, awaiting further analysis.

In Fig. 1 the line shapes of the individual vibration-rotation-translation lines have been chosen as being Lorentzian with HWHHs equal to 24 cm^{-1}, while those of the small sharp features have been chosen as being 14 cm^{-1}. The Lorentz shapes of the broader features would presumably result from coherence loss due to random perturbations of the vibration-rotation-translation states by thermal fluctuations. The sharper features do not suffer loss of coherence due to interactions with translational motions and hence have narrower shapes. The broad spectra do not appear to be overly sensitive to the linewidths, say, for variations within ±10%.

On the basis of the transition dipole moments described above, we have calculated the maximum radiative absorption, at 4220 cm^{-1}, through standard quantum mechanical techniques. Using the index of refraction 1.95 (Ref. 27) and the individual component linewidths of 24 cm^{-1} we find the absorption constant to be 0.06 cm^{-1}. To give a typically observed[27] fractional absorption of 7% the mean path length of diffusing radiation within the sample would be about 1.2 cm. In view of the typical sample sizes used, this figure seems to be reasonable. However, an accurate value for this length is not known so that quantitative comparison with experiment is not possible at this time.

Finally, it is useful to investigate the effects of two different sets of assumptions on the theoretical line shape:

(i) use of a Gaussian line profile for each component of the spectrum rather than a Lorentzian; and

(ii) the use of the Lennard-Jones potential, rather than an exp-6 potential. The use of Gaussian profiles leads to the theoretical spectrum of Fig. 4. This would be the better model *if* the principal causes of line broadening were that individual lines were not true singlets as would be the case with the separation model, but were split according to the

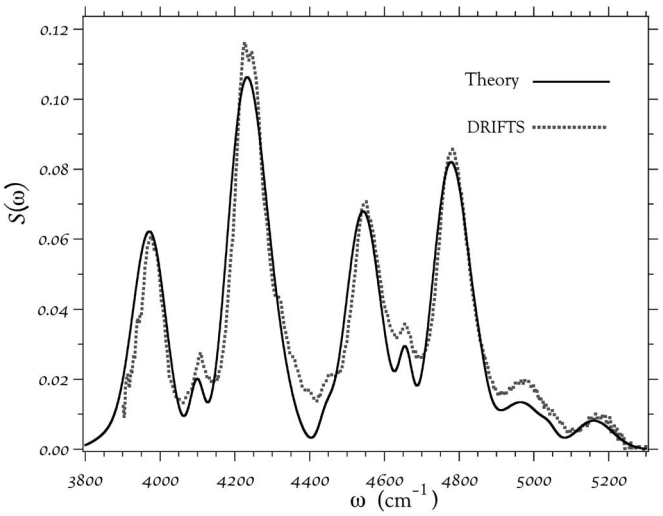

FIG. 4. Theoretical spectrum using Gaussian line shapes. The width parameters are the same as for the Lorentzian fit of Fig. 1.

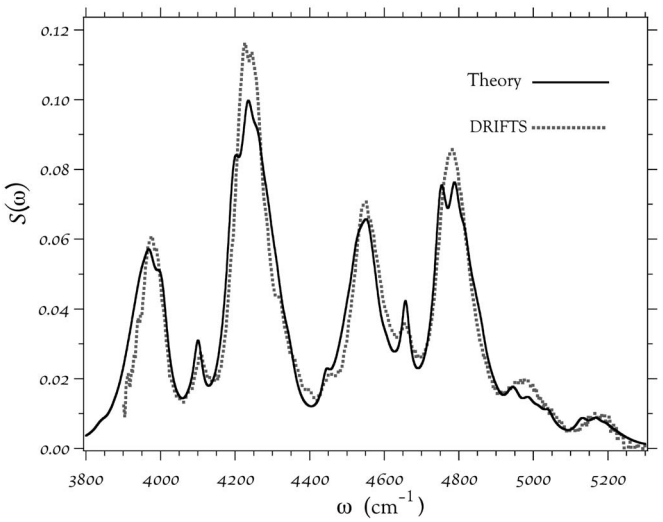

FIG. 5. Theoretical spectrum using a Lennard-Jones interaction, with the same σ and ε as used for the exp-6 potential in Fig. 1.

small energy differences between the exact and the separable potential, and also the small splittings which result from anisotropic interactions between H_2 and the C_{60} lattice. Such sources of linewidth are inhomogeneous—that is, they result from a large variety of inequivalent static or slowly varying perturbations of the H_2 molecules. In homogeneous line broadening, on the other hand, which characteristically gives Lorentzian line shapes, stochastic time-dependent interactions perturb each microsituation equally to give the line shape, and homogeneously broadened lines are more or less Lorentzian. The obvious problem with the Gaussian profiles is that the wings of the principal broad features are not strong enough to account successfully for the valleys between the large peaks, whereas Lorentzian line shapes are successful. Hence it appears that the lines are largely homogeneously perturbed, presumably from some combination of lattice vibrations, and rotation of the C_{60} molecules.

In Fig. 5 we show our best Lennard-Jones spectrum, for which $\sigma=3.20$ Å and $\varepsilon=3.25$ meV. An unavoidable flaw in Lennard-Jones 12-6 potentials, as models for the C-H_2 interaction in C_{60}, is that the hardness of the repulsive parts of their interactions leads to major peaks which are too broad and/or split, which is not in accord with observation. We note that the spectra resulting from Lennard-Jones interactions tend toward those of a particle in a box, as a result of the hard repulsive part of the potentials. The translational peaks are more widely split than they are in the softer potential provided by the exponential short range interaction.

The spectra resulting from Lennard-Jones interactions are, as a result of the hard repulsive part, closer to those of a particle in a box, in which the translational peaks are more widely split than they are in the softer potential provided by the exponential short range force which, itself, gives well potentials which more closely resemble an isotropic harmonic oscillator, for which the transition energies are equal.

VIII. SUMMARY, DISCUSSION, AND CONCLUSIONS

From the comparison of calculated and observed spectra, as in Fig. 1, we conclude that the best values of σ and ε are 3.22 Å and 3.25 meV, for the choice of the β parameter as described above. We have not yet carried out a systematic sampling of all combinations of σ and ε around the above values, the cases that we have examined reveal that σ lies within 1% of the above value, while ε is less tightly constrained. It turns out that within the present parametrization, the spectrum is not so very dependent upon the detailed magnitudes of the various dipole components, provided that γ is properly selected. Far more important is the distribution of energy differences between the successive translational states. The exp-6 potentials, even for other values of β, in general can give good distributions of the energy differences, for the best choices of σ and ε.

If the agreement between observed and calculated spectra were all there were to this problem, we might regard this problem as being closed. But there are other aspects to the problem that are not in such good order, at the moment. Among other things, FitzGerald *et al.* have measured the absorption energy for H_2 in the C_{60} lattice, and have concluded that this energy is 1058 K, though they did allow that some correction to this value might eventually be found. For our part, we can calculate this energy through two possible means. The resulting numbers can give us some meaningful ideas on the validity of classical positional distributions (as we have used them for describing the motions transverse to the z direction throughout), as compared with totally quantum mechanical treatment of these degrees of freedom. In the classical form, we could simply say that the absorption energy is

$$E_{\mathrm{abs}} = -Q_{3\mathrm{D}}^{-1} \int dxdydzV(x,y,z)e^{-V(x,y,z)/k_BT}, \qquad (48)$$

where $Q_{3\mathrm{D}}$ is given by Eq. (40). In the separable potential approximation this becomes

$$E_{\mathrm{abs}} = 3\left(-Q^{-1} \int dxV_{1\mathrm{D}}(x)e^{-V_{1\mathrm{D}}(x)/k_BT}\right) \qquad (49)$$

with Q given by Eq. (41). Using Eq. (49) with our best C_{60}-H_2 potential gives $E_{\mathrm{abs}}=1302$ K.

The quantum mechanical form of Eq. (48) is

$$E_{\mathrm{abs}} = \frac{3}{2}k_B T - Z_{3\mathrm{D}}^{-1} \sum_{n_x n_y n_z} E_{n_x n_y n_z} e^{-E_{n_x n_y n_z}/k_B T}, \qquad (50)$$

where $Z_{3\mathrm{D}}$ is given by Eq. (39). The first term in Eq. (50) gives the mean energy of the free molecule, to which the bound state energies would have to be raised in desorption. In the separable potential approximation, Eq. (50) becomes

$$E_{\mathrm{abs}} = 3\left(\frac{k_B T}{2} - Z^{-1}\sum_n E_n e^{-E_n/k_B T}\right). \qquad (51)$$

From Eq. (51) we obtain $E_{\mathrm{abs}}=1329$ K, which differs only by about 2% from the classical value, each of which differ by some 25% from the value quoted by Fitzgerald *et al.*

One might envision some further parametrization, perhaps through variation of β, together with σ and ε, to improve this agreement while preserving the good agreement between the calculated and observed spectra, were it not for another somewhat troubling factor. That is, if one uses the bond polarizabilities referred to above to calculate the long range force constant C_6 through the London procedure,[22–24] this constant is found to be given by the expression

$$C_6 = \alpha_{\mathrm{H_2}}\left(\frac{2\alpha_{\perp s}+\alpha_{\parallel s}}{2} + \frac{2\alpha_{\perp d}+\alpha_{\parallel d}}{4}\right)\left(\frac{I_{\mathrm{H_2}} I_{\mathrm{C}}}{I_{\mathrm{H_2}} + I_{\mathrm{C}}}\right) \qquad (52)$$

the value of which is 26.9 a.u. The value given by the exp-6 potential with $\sigma=3.22$ Å and $\varepsilon=3.25$ meV is 25.6. This appears to give reasonable agreement, except for the following considerations. More recent values[25] for C_6 are routinely 10 to 20% higher than the London values, which widens the discrepancy, and available bond polarizability data,[26] while incomplete, appear to suggest higher bond polarizabilities for C_{60} than given by the organic molecular bond polarizabilities, which again would widen the discrepancy. The problem that one may ultimately face is how to lower the absorption energy while increasing the depths of the wells. Finally, the value of ε calculated by Pradhan *et al.*[2] for distorted carbon structures in which the carbon resonant structure of the bonds has been destroyed, as is the case with C_{60}, appears to be considerably greater than that which we have found to give good spectra.

We have demonstrated that the DRIFT spectra strongly constrain the C-H_2 potential needed to obtain them. Similarly the relative intensities of the DRIFTS lines constrain models for the C_{60}-H_2 induced dipole, up to a multiplicative constant. In particular the parameter γ relating the short range and the long range part of the induced dipole is constrained, and the principal feature widths, the shapes of the valleys and the shapes of the sharks' teeth yield information about the homogeneous linewidths. All in all, we have demonstrated that a simple model for the C_{60}-H_2 interaction can give excellent agreement with observation.

We think that the considerable differences which we find between the C-H_2 potential in fullerite and C-H_2 potentials found in graphene[11,15,19,20] are reflective of the differences in bonding between these two systems,[12] as is reflected in their very different chemistries.[12]

Progress in refining our present model would be facilitated through more certain knowledge of the H_2 absorption energy, bond polarizabilities for C_{60}, and the ε value for C_{60}-H_2. Nonetheless, it is doubtful that any better interaction which may in the future be developed will differ too significantly from the exp-6 potential with the values $\sigma=3.22$ Å (hence $\beta=3.5066$ Å^{-1}) and $\varepsilon=3.25$ meV which we have demonstrated in the present work to produce good agreement with spectroscopic results.

ACKNOWLEDGMENTS

We thank S. A. FitzGerald for permission to use his DRIFTS data in Figs. 1–5, for several extensive discussions, and for his comments on earlier drafts of this paper. We acknowledge useful discussions on graphene and carbon nanostructures with M. W. Cole, P. C. Eklund, and V. Crespi. One of us (R.M.H.) gratefully acknowledges support from the Fulbright Foundation, and thanks the Department of Physics and Physical Oceanography of the Memorial University of Newfoundland for its hospitality for several months in 2001–2003, both of which facilitated this work. One of us (J.C.L.) thanks the Department of Physics of the Pennsylvania State University for its hospitality in 1999–2000 and in 2005, and acknowledges support from the Natural Sciences and Engineering Research Council of Canada.

*Electronic address: rmh@hbar.phys.psu.edu

†Electronic address: court@physics.mun.ca

[1] S. A. FitzGerald, S. Forth, and M. Rinkoski, Phys. Rev. B **65**, 140302(R) (2002).

[2] B. K. Pradhan, A. R. Harutyunyan, D. Stojkovic, J. Grossman, P. Zhang, M. W. Cole, V. Crespi, H. Goto, J. Fujiwara, and P. C. Eklund, J. Mater. Res. **17**, 2209 (2002).

[3] R. M. Herman and J. C. Lewis, in *Proceedings of the 17th International Conference on Spectral Line Shapes*, edited by E. Dalimier (Frontier Group, 2004), pp. 369–371.

[4] R. M. Herman and J. C. Lewis, in *Spectral Line Shapes Volume 12*, edited by C. Back, AIP Conf. Proc. No. 645 (AIP, New York, 2002), pp. 233–236.

[5] L. Frommhold, *Collision-Induced Absorption in Gases* (Cambridge University Press, Cambridge, 1993).

[6] M. S. Dresselhaus, G. Dresselhaus, and P. C. Eklund, *Science of Fullerenes and Carbon Nanotubes* (Academic Press, New York, 1996).

[7] S. A. FitzGerald, T. Yildirim, L. J. Santodonato, D. A. Neumann, J. R. D. Copley, J. J. Rush, and F. Trouw, Phys. Rev. B **60**, 6439 (1999).

[8] S. A. FitzGerald, R. Hannachi, D. Sethna, M. Rinkoski, K. K.

Sieber, and D. S. Sholl, Phys. Rev. B **71**, 045415 (2005).
[9] A. Borysow, L. Frommhold, and W. Meyer, J. Comp. Physiol. **88**, 4855 (1988).
[10] J. C. Phillips, *Covalent Bonding in Crystals, Molecules, and Polymers* (University of Chicago Press, Chicago, 1969).
[11] A. D. Novaco, Phys. Rev. Lett. **60**, 2058 (1988).
[12] A. Hirsch and M. Brettreich, *Fullerenes—Chemistry and Reactions* (WILEY-VCH, 2005).
[13] J. Schaefer and W. E. Kohler, Physica A **129**, 469 (1985).
[14] R. J. LeRoy and J. S. Carlin, *Spectroscopy and Potential Energy Surfaces of van der Waals Molecules* (Interscience, Oxford, 1980), Vol. 17, pp. 353–420.
[15] S. C. Wang, L. Sembetu, and C. W. Woo, J. Low Temp. Phys. **41**, 611 (1980).
[16] T. Yildirim and A. B. Harris, Phys. Rev. B **66**, 214301 (2002).
[17] R. M. Herman and S. Short, J. Chem. Phys. **48**, 1266 (1968).
[18] J. D. Poll and J. L. Hunt, Can. J. Phys. **54**, 461 (1976).
[19] A. D. Novaco and J. P. Wroblewski, Phys. Rev. B **39**, 11364 (1989).
[20] A. D. Novaco, Phys. Rev. B **46**, 8178 (1992).
[21] K. A. Williams, B. Pradhan, P. C. Eklund, M. K. Kostov, and M. W. Cole, Phys. Rev. Lett. **88**, 165502 (2002).
[22] F. London, Z. Phys. **63**, 245 (1930).
[23] F. London, Z. Phys. Chem. Abt. B **11**, 222 (1930).
[24] H. Margenau and N. R. Kestner, *Theory of Intermolecular Forces* (Pergamon Press, New York, 1969), pp. 32–33.
[25] A. E. Kingston, Phys. Rev. **135**, A1018 (1964).
[26] D. W. Snoke, M. Cardona, S. Sanguinetti, and G. Benedek, Phys. Rev. B **53**, 12641 (1996), and references therein.
[27] S. A. FitzGerald (private communication).